

Relativistic non-Fermi liquid fixed point in (2+1)-dimensional birefringent Dirac fermions interacting with electromagnetic fields

Wan-Zi Sun(孙万梓), Kai Liu(刘恺), Wu-Ming Liu(刘伍明), and Cheng-Xi Li(李成蹊)

Citation : Chin. Phys. B, 2025, 34 (**5**): 057102. DOI: 10.1088/1674-1056/adb9cd
http://cpb.iphy.ac.cn; http://iopscience.iop.org/cpb

What follows is a list of articles you may be interested in

Single crystal growth and electronic structure of Rh-doped $Sr_3Ir_2O_7$

Bingqian Wang(王冰倩), Shuting Peng(彭舒婷), Zhipeng Ou(欧志鹏), Yuchen Wang(王宇晨), Muhammad Waqas, Yang Luo(罗洋), Zhiyuan Wei(魏志远), Linwei Huai(淮琳崴), Jianchang Shen(沈建昌), Yu Miao(缪宇), Xiupeng Sun(孙秀鹏), Yuewei Yin(殷月伟), and Junfeng He(何俊峰)
Chin. Phys. B, 2023, 32 (**8**): 087108. DOI: 10.1088/1674-1056/acd7d5

Symmetry-constrained quantum coupling in non-Fermi-liquid transport

Rong Li(李荣) and Zhen-Su She(佘振苏)
Chin. Phys. B, 2023, 32 (**6**): 067104. DOI: 10.1088/1674-1056/acc0f4

A sport and a pastime: Model design and computation in quantum many-body systems

Gaopei Pan(潘高培), Weilun Jiang(姜伟伦), and Zi Yang Meng(孟子杨)
Chin. Phys. B, 2022, 31 (**12**): 127101. DOI: 10.1088/1674-1056/aca083

Global phase diagram of a spin-orbit-coupled Kondo lattice model on the honeycomb lattice

Xin Li(李欣), Rong Yu(俞榕), Qimiao Si
Chin. Phys. B, 2019, 28 (**7**): 077102. DOI: 10.1088/1674-1056/28/7/077102

Phase diagram, correlations, and quantum critical point in the periodic Anderson model

Jian-Wei Yang(杨建伟), Qiao-Ni Chen(陈巧妮)
Chin. Phys. B, 2018, 27 (**3**): 037101. DOI: 10.1088/1674-1056/27/3/037101

Relativistic non-Fermi liquid fixed point in (2+1)-dimensional birefringent Dirac fermions interacting with electromagnetic fields

Wan-Zi Sun(孙万梓)[1,2], Kai Liu(刘恺)[1,2], Wu-Ming Liu(刘伍明)[1,2,3], and Cheng-Xi Li(李成蹊)[1,2,†]

[1] *Beijing National Laboratory for Condensed Matter Physics and Institute of Physics, Chinese Academy of Sciences, Beijing* 100190, *China*
[2] *School of Physical Sciences, University of Chinese Academy of Sciences, Beijing* 100190, *China*
[3] *Songshan Lake Materials Laboratory, Dongguan* 523808, *China*

(Received 30 December 2024; revised manuscript received 25 February 2025; accepted manuscript online 25 February 2025)

The system consisting of (2+1)-dimensional quasirelativistic birefringent Dirac fermions with Coulomb interactions and retarded current–current interactions is described by a quantum field theory similar to reduced quantum electrodynamics. We used the perturbative renormalization group method to study the low-energy behavior of the system and found that it flows to a fixed point of the non-Fermi liquid composed of relativistic pseudospin-1/2 Dirac fermions in the deep infrared limit. At the fixed point, the fermion Green function exhibits a finite anomalous dimension, and the residue of the quasiparticle pole vanishes in a power-law fashion. Our research provides new theoretical perspectives for understanding the origin of spin-1/2 fermions in the standard model.

Keywords: non-Fermi liquid fixed point, birefringent Dirac fermions, perturbative renormalization group, Fermi velocity renormalization

PACS: 71.10.Hf, 11.10.Hi

DOI: 10.1088/1674-1056/adb9cd **CSTR:** 32038.14.CPB.adb9cd

1. Introduction

In recent years, quantum critical phenomena have become one of the most intriguing research topics in condensed matter physics.[1–7] On the other hand, higher spin fermions have been hypothesized as emergent quasiparticles in solid-state systems near band-touching points, such as pseudospin-3/2 fermions emerge near linear band-touching points, where quasiparticles exhibit a birefringent spectrum with two different Fermi velocities, breaking Lorentz symmetry. These fermions can be realized in systems such as tight-binding models on generalized π-flux square lattices.[8–12]

Reduced quantum electrodynamics (RQED), also known as pseudoquantum electrodynamics (PQED), is the correct approach for introducing U(1) gauge fields in planar materials. It is a mixed-dimensional quantum field theory that describes 2+1 fermions interacting with a (3+1)-dimensional electromagnetic field. RQED/PQED has gained increasing attention in both theoretical[13–17] and numerical researches,[18] PQED eliminates the logarithmic divergence of the Coulomb potential in QED3, providing the correct Coulomb potential $V(r) \propto 1/r$ in the static limit and accurately describing electron–electron interactions in two-dimensional (2D) materials. In the context of RQED, the renormalization of the Fermi velocity has also been investigated.[19,20]

In this paper, we extend reduced quantum electrodynamics to reduced quantum electrodynamics for birefringent Dirac fermions, a theory describing the interaction between (2+1)-dimensional birefringent Dirac fermions and a (3+1)-dimensional electromagnetic field. Using the perturbative renormalization group method, we investigate the low-energy behavior of the system. In the deep infrared region, the quasi-relativistic birefringent Dirac fermions degrade into two decoupled relativistic pseudospin-1/2 Dirac fermions and exhibit non-Fermi liquid behavior. Our paper is organized as follows. In Section 2, we propose an optical lattice experiment to realize a tight-binding model that gives rise to birefringent Dirac fermions in the low-energy limit. We also introduce the model for the interaction between birefringent Dirac fermions and the electromagnetic field. In Section 3, we calculate the one-loop perturbative corrections to this model. In Section 4, we perform a renormalization group flow analysis and discuss the two limits of our theory. At last we will give the summation of our paper.

2. Model and experiment

The birefringent Dirac fermions arise from the low-energy limit of the following tight-binding model:[8]

$$\begin{aligned}\hat{H} = & -J_0 \sum_{x,y} \left[\left(1+\beta\, \mathrm{e}^{\pi \mathrm{i} x}\right) c^{\dagger}_{x,y+1} c_{x,y} + \text{h.c.} \right] \\ & + \left[\left(\beta + \mathrm{e}^{\pi \mathrm{i} y}\right) c^{\dagger}_{x+1,y} c_{x,y} + \text{h.c.} \right]. \end{aligned} \tag{1}$$

This Hamiltonian is obtained from the spin-independent hopping of fermions on a generalized π-flux square lattice.[8] Here J_0 is the primary hopping amplitude, β is the dimensionless

†Corresponding author. E-mail: lcxtom@icloud.com

© 2025 Chinese Physical Society and IOP Publishing Ltd. All rights, including for text and data mining, AI training, and similar technologies, are reserved.

birefringent parameter, and $c^{\dagger}_{x,y}$ ($c_{x,y}$) creates (annihilates) an electron at site (x,y). The phase factors $e^{\pi i x}$ and $e^{\pi i y}$ introduce a staggered pattern in the hopping amplitudes.

Before we discuss in detail the birefringent fermions and their interactions, let us propose an experimental scheme different from that in Ref. [8] to realize this tight-binding Hamiltonian.

A systematic scheme is presented for realizing time-modulated tunneling of spinless fermions in optical lattices. As shown in Fig. 1(a), our experimental apparatus consists of a three-dimensional (3D) optical lattice created by three mutually orthogonal standing waves with wavelengths $\lambda_{x,y} = 767$ nm and $\lambda_z = 844$ nm, yielding lattice constants $d_i = \lambda_i/2$. To achieve an effective 2D system, we employ a deep lattice potential ($V_z = 30E_{rz}$) along the vertical direction to suppress the inter-plane tunneling. Within the xy plane, we initially configure the lattice with depths $V_x = 5.0E_r$ and $V_y = 40E_r$, where the latter effectively inhibits spontaneous tunneling along y. The time-modulated tunneling is implemented using a magnetic field gradient $B' = 17.5$ mGs/μm (1 Gs = 10^{-4} T) along x and a pair of running-wave beams ($\lambda_K = 2\lambda_y$, $\omega = \Delta/\hbar$, $V_K^0 = 9.9E_{rK}$) to restore resonant tunneling. The tunneling along y is controlled by periodic modulation of the lattice depth.

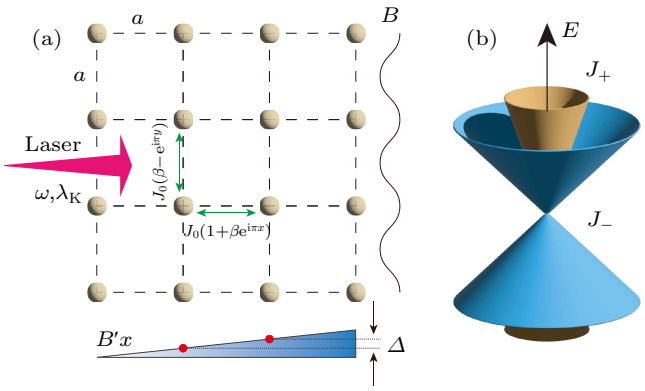


Fig. 1. Schematic illustration of the experimental setup. (a) Three-dimensional (3D) optical lattice formed by orthogonal standing waves with wavelengths $\lambda_{x,y} = 767$ nm and $\lambda_z = 844$ nm, and lattice depths are set to $V_x = 5.0E_r$, $V_y = 40E_r$. Time-modulated tunneling is implemented using a magnetic field gradient $B' = 17.5$ mGs/μm along x and a pair of running-wave beams ($\lambda_K = 2\lambda_y$, $\omega = \Delta/\hbar$, $V_K^0 = 9.9E_{rK}$) to restore resonant tunneling. The tunneling along y is controlled by periodic modulation of the lattice depth. (b) Near half-filling, the system exhibits a single inequivalent Dirac point (in contrast to graphene's two), where two Dirac cones emerge with distinct Fermi velocities $2J_+$ and $2J_-$, where $J_\pm = J_0\,(1\pm\beta)$ and β is the dimensionless birefringent parameter. The low-energy physics is governed by gapless birefringent Dirac fermion excitations characterized by these distinct velocities.

Under periodic modulation with period t_0 of the laser field along x direction, the system dynamics can be described by an effective time-independent Hamiltonian.[8,21,22] The Hamiltonian takes the form $\hat{H} = -J_0\sum_{x,y}[(1+\beta\,e^{\pi i x})c^{\dagger}_{x,y+1}c_{x,y} + (\beta + e^{\pi i y})c^{\dagger}_{x+1,y}c_{x,y} + \text{h.c.}\,]$, where J_0 represents the primary hopping amplitude determined by the bare tunneling rate, and β is a dimensionless birefringent parameter that can be continuously tuned through the modulation depth of the lattice potential. The operators $c^{\dagger}_{x,y}$ and $c_{x,y}$ create and annihilate fermions at site (x,y), respectively. The phase factors $e^{\pi i x}$ and $e^{\pi i y}$ emerge from the interplay between the magnetic field gradient and the running-wave beams, introducing a staggered pattern in the hopping amplitudes. This spatial modulation of both the magnitude and phase of the hopping terms distinguishes our model from previous studies of particles in periodic magnetic fields.

Let us return to the tight-binding Hamiltonian (1), in momentum space near half-filling, expanding around the Dirac point and keeping terms up to linear order in momentum, the low-energy effective Hamiltonian takes the form $H_{BF}(\boldsymbol{k}) = v(\Gamma_{13}k_1 + \Gamma_{01}k_2) + \beta v(\Gamma_{10}k_1 + \Gamma_{31}k_2)$,[8] where $v = 2J_0a$ (with a being the lattice constant),$v > 0$, and $\Gamma_{\mu\nu} = \sigma_\mu \otimes \sigma_\nu$ are the gamma matrices with $\mu,\nu = 0,1,2,3$. Here σ_0 is the 2×2 unity matrix, and $\sigma_{1,2,3}$ are the Pauli matrices, the eigenvalues of this Hamiltonian are $\pm E^{\pm}_{BF}(\boldsymbol{k})$ and $E^{\pm}_{BF}(\boldsymbol{k}) = (1\pm\beta)v|\boldsymbol{k}| = v_\pm|\boldsymbol{k}|$, here $v_\pm = (1\pm\beta)v$ represents the effective Fermi velocity, where β is the birefringent parameter, the energy spectrum is shown in Fig. 1(b), when $\beta = 0$, the system corresponds to two degenerate pseudospin-1/2 fermions, when $\beta = 1/2$, it is equivalent to pseudospin-3/2 fermions, and when $\beta = 1$, it corresponds to two flat bands and a Dirac cone, similar to the Lieb lattice.[23] We restrict β to $0 \le \beta < 1$, but later, by defining $w = \beta v$, we can extend β to values greater than 1. Through a unitary transformation $U^{\dagger}H_{BF}(\boldsymbol{k})U \to H_{BF}(\boldsymbol{k})$, with $U = e^{i\frac{\pi}{4}\Gamma_{23}}e^{i\frac{\pi}{4}\Gamma_{32}}e^{-i\frac{\pi}{4}\Gamma_{30}}e^{i\frac{\pi}{4}\Gamma_{20}}e^{i\frac{\pi}{4}\Gamma_{01}\Gamma_{22}}$[24] the Hamiltonian can be transformed into a more symmetry form[25]

$$\begin{aligned} H_{BF}(\boldsymbol{k}) &= H_1(\boldsymbol{k}) + \beta H_2(\boldsymbol{k}) \\ &= v(\Gamma_{10}k_1 + \Gamma_{20}k_2) + \beta v(\Gamma_{01}k_1 + \Gamma_{02}k_2), \end{aligned} \tag{2}$$

where $H_1(\boldsymbol{k}) = v(\Gamma_{10}k_1 + \Gamma_{20}k_2)$, $H_2(\boldsymbol{k}) = v(\Gamma_{01}k_1 + \Gamma_{02}k_2)$. This transformation does not alter any properties of the birefringent fermions, except that it makes the subsequent calculations more convenient. So far, we have considered the free theory of birefringent Dirac fermions. Next, we introduce the interactions between the birefringent Dirac fermions, considering both Coulomb interactions and retarded current–current interactions (The case considering only Coulomb interactions has already been studied in Ref. [25]).

We begin with the following imaginary-time action:

$$S = \int d^2x\,d\tau\,\mathcal{L}_{BF} + \int d^3x\,d\tau\,\mathcal{L}_{EM}, \tag{3}$$

where $\mathcal{L}_{BF}$ includes the free Lagrangian of the birefringent fermions and the interaction Lagrangian between the birefringent fermions and the electromagnetic field, and $\mathcal{L}_{EM}$ is the electromagnetic field Lagrangian in 3D space,

$$\mathcal{L}_{BF} = \Psi^{\dagger}\left[\partial_\tau - ieA_0 + H_{BF}\left(\boldsymbol{k} \to -i\boldsymbol{\nabla} - \frac{e}{c}\boldsymbol{A}\right)\right]\Psi,$$

$$\mathcal{L}_{\rm EM} = \frac{1}{4}F_{\mu\nu}F_{\mu\nu} + \frac{1}{2\xi}(\partial_\mu A_\mu)^2, \tag{4}$$

where e is the electronic charge, and the speed of light c in the material is related to its electromagnetic properties through $c = c_0/\sqrt{\varepsilon\mu}$, with c_0 being the speed of light in a vacuum, and ε and μ are the permittivity and permeability of the medium, respectively. Here, $\Psi^\dagger$ and Ψ are two independent Grassmann variables. Where $\mu,\nu = 0,1,2,3$ and $\partial_\tau = c\partial_0$, $\omega = ck_0$ and $F_{\mu\nu} = \partial_\mu A_\nu - \partial_\nu A_\mu$ is the electromagnetic field strength tensor. ξ is the gauge fixing parameter. The dynamics of birefringent Dirac fermions is set by the fermionic Green's function[24–26]

$$G(\mathrm{i}\omega,\boldsymbol{k}) = \frac{1}{\mathrm{i}\omega + H_{\rm BF}(\boldsymbol{k})} = \frac{[-\mathrm{i}\omega + H_{\rm BF}(\boldsymbol{k})][\omega^2 + (1+\beta^2)v^2|\boldsymbol{k}|^2 - 2\beta v^2 H_1(\boldsymbol{k})H_2(\boldsymbol{k})]}{[\omega^2 + (1+\beta)^2v^2|\boldsymbol{k}|^2][\omega^2 + (1-\beta)^2v^2|\boldsymbol{k}|^2]}. \tag{5}$$

The electromagnetic field propagator in (3+1) dimensions is given by[27]

$$D_{\mu\nu}(\mathrm{i}\omega,\boldsymbol{k}) = \frac{1}{\varepsilon k^2}\left[\delta_{\mu\nu} - (1-\xi)\frac{k_\mu k_\nu}{k^2}\right], \tag{6}$$

where $k^2 = \omega^2/c^2 + k_1^2 + k_2^2 + k_3^2$, here ω is the Matsubara frequency, when $\mu = \nu$, $\delta_{\mu\nu} = 1$, and when $\mu \neq \nu$, $\delta_{\mu\nu} = 0$. In the reduced space where the fermions live, the reduced electromagnetic field propagator $\tilde{D}_{\mu_{\rm e}\nu_{\rm e}}(\mathrm{i}\omega,\boldsymbol{k}_{\rm e})$ is[20,28,29]

$$\begin{aligned}\tilde{D}_{\mu_{\rm e}\nu_{\rm e}}(\mathrm{i}\omega,\boldsymbol{k}_{\rm e}) &= \int_{-\infty}^{\infty}\frac{\mathrm{d}k_3}{2\pi}D_{\mu_{\rm e}\nu_{\rm e}}(\mathrm{i}\omega,\boldsymbol{k}) \\ &= \frac{1}{2\varepsilon\sqrt{k_{\rm e}^2}}\left[\delta_{\mu_{\rm e}\nu_{\rm e}} - \frac{(1-\xi)}{2}\frac{k_{\mu_{\rm e}}k_{\nu_{\rm e}}}{k_{\rm e}^2}\right],\end{aligned} \tag{7}$$

where $\mu_{\rm e}$, $\nu_{\rm e} = 0,1,2$ are the indices for the (2+1)-dimensional birefringent Dirac fermions, $k_{\rm e}^2 = \omega^2/c^2 + k_1^2 + k_2^2$. In the one loop perturbation calculation in the next section, for convenience, we will ignore the fermion subscript e and use the Feynman gauge $\xi = 1$. The interaction vertex between birefringent Dirac fermions and photons is given by $e\gamma_\mu$, where $\mu = 0,1,2$ and

$$\gamma_\mu = \left[\mathrm{i},\ \frac{v}{c}(\Gamma_{10} + \beta\Gamma_{01}), \frac{v}{c}(\Gamma_{20} + \beta\Gamma_{02})\right]. \tag{8}$$

3. One loop perturbation calculation

The quantum corrections to the birefringent fermion propagator can be systematically analyzed using dimensional regularization in $D = 2-\epsilon$ dimensions and minimal subtraction renormalization scheme.[30] The Feynman diagram for the birefringent fermion one-loop self-energy correction is shown in Fig. 2(a). Following standard field-theoretical techniques and after extensive algebraic manipulations, we obtain the one-loop self-energy correction

$$\begin{aligned}\Sigma(\mathrm{i}\Omega,\boldsymbol{p}) &= e^2\int\frac{\mathrm{d}^Dk}{(2\pi)^D}\int\frac{\mathrm{d}\omega}{2\pi}\gamma_\mu G(\mathrm{i}\omega,\boldsymbol{k})\gamma_\nu\tilde{D}_{\mu\nu}(\mathrm{i}\Omega - \mathrm{i}\omega,\boldsymbol{p}-k) \\ &= \frac{3g^2}{16\pi^2 c}\left[\frac{1}{\epsilon} + O(\epsilon^0)\right]\int_0^1\mathrm{d}x\int_0^{1-x}\mathrm{d}y\frac{\sqrt{1-x-y}}{f(x,y)}\left\{\frac{2\beta\frac{v^2}{c^2}}{3f(x,y)}\left[4\beta\frac{v^2}{c^2}(1+\Gamma_{33}) - (\Gamma_{11}+\Gamma_{22})\right](\mathrm{i}\Omega)\right. \\ &\quad + \left[1 + \frac{2(1+\beta^2)\frac{v^2}{c^2}}{3f(x,y)}\right]\left[1 - 2(1+\beta^2)\frac{v^2}{c^2} - 2\beta\frac{v^2}{c^2}(\Gamma_{11}+\Gamma_{22})\right](\mathrm{i}\Omega) \\ &\quad \left. - \left[\frac{1-4\beta^2\frac{v^2}{c^2}}{3f(x,y)} + \frac{4(1-\beta^2)\frac{v^2}{c^2}}{3f^2(x,y)}\right]v(\Gamma_{10}p_1 + \Gamma_{20}p_2) - \left[\frac{1-4\frac{v^2}{c^2}}{3f(x,y)} - \frac{4(1-\beta^2)\frac{v^2}{c^2}}{3f^2(x,y)}\right]v\beta(\Gamma_{01}p_1 + \Gamma_{02}p_2)\right\}.\end{aligned} \tag{9}$$

where $f(x,y) = 1 - x[1-(1+\beta)^2v^2/c^2] - y[1-(1-\beta)^2v^2/c^2]$, $g^2 \equiv e^2/\varepsilon$, the counterterm of the birefringent fermionic self-energy can be written as

$$\Sigma_{\rm ct}(\mathrm{i}\Omega,\boldsymbol{p}) = -(Z_\Psi - 1)\mathrm{i}\Omega - (Z_\Psi Z_v - 1)v(\Gamma_{10}p_1 + \Gamma_{20}p_2) - (Z_\Psi Z_v Z_\beta - 1)v\beta(\Gamma_{01}p_1 + \Gamma_{02}p_2). \tag{10}$$

According to the minimal subtraction renormalization scheme, we obtain the following renormalization constants:

$$Z_\Psi = 1 + \frac{3g^2}{16\pi^2 c}\frac{1}{\epsilon}\int_0^1\mathrm{d}x\int_0^{1-x}\mathrm{d}y\frac{\sqrt{1-x-y}}{f(x,y)}\left[1 - 2(1+\beta^2)\frac{v^2}{c^2} + \frac{2(1+\beta^2)\frac{v^2}{c^2} - 4(1+\beta^4)\frac{v^4}{c^4}}{3f(x,y)}\right], \tag{11}$$

$$Z_v = 1 - \frac{3g^2}{16\pi^2 c}\frac{1}{\epsilon}\int_0^1\mathrm{d}x\int_0^{1-x}\mathrm{d}y\frac{\sqrt{1-x-y}}{f(x,y)}\left[1 - 2(1+\beta^2)\frac{v^2}{c^2} + \frac{1+2(1-\beta^2)\frac{v^2}{c^2} - 4(1+\beta^4)\frac{v^4}{c^4}}{3f(x,y)} + \frac{4(1-\beta^2)\frac{v^2}{c^2}}{3f^2(x,y)}\right], \tag{12}$$

$$Z_\beta = 1 + \frac{3g^2}{16\pi^2 c}\frac{1}{\epsilon}\int_0^1\mathrm{d}x\int_0^{1-x}\mathrm{d}y\frac{\sqrt{1-x-y}}{f(x,y)}\left[\frac{4(1-\beta^2)\frac{v^2}{c^2}}{3f(x,y)} + \frac{8(1-\beta^2)\frac{v^2}{c^2}}{3f^2(x,y)}\right]. \tag{13}$$

The calculation of the vertex correction [Fig. 2(b)] and the proof of the Ward identity are placed in Appendix A. The validity of the Ward identity leads to $Z_{\rm e}Z_{\rm A}^{1/2}=1$, and ensures that the fermion velocity renormalization constant Z_v obtained from the fermion self-energy diagram is equal to the one obtained from the vertex correction.[19] It also guarantees that the renormalization constant Z_β for the birefringent parameter, calculated from both Feynman diagrams [Figs. 2(a) and (b)], is the same. We then have the nice situation of dealing with a nonrelativistic quantum field theory in which the Fermi velocity of the electrons and the birefringent parameter is renormalized exactly in the same way in the different terms of the action.

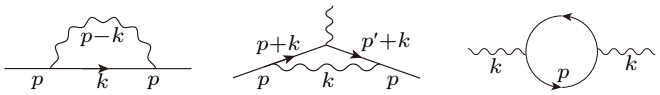


Fig. 2. Leading-order (one-loop) Feynman diagrams, the solid lines with arrows represent the propagator of the birefringent Dirac fermions, while the wavy lines represent the photon propagator. (a) Self-energy correction for birefringent Dirac fermions, (b) vertex correction, and (c) photon self-energy correction.

Photon self-energy correction [see Fig. 2(c)] in (2+1) dimensions reads as

$$\begin{aligned}&\Pi_{\mu\nu}(\mathrm{i}\omega,\boldsymbol{k})\\&=-e^2\int\frac{\mathrm{d}^2\boldsymbol{p}}{(2\pi)^2}\int_{-\infty}^{\infty}\frac{\mathrm{d}\Omega}{2\pi}\\&\quad\times\mathrm{Tr}\left[\gamma_\mu G(\mathrm{i}\Omega,\boldsymbol{p})\gamma_\nu G(\mathrm{i}\Omega+\mathrm{i}\omega,\boldsymbol{p}+\boldsymbol{k})\right].\end{aligned}\tag{14}$$

This integral is linearly divergent, and in dimensional regularization, the divergent part appears in the values of the Gamma function at zero and negative integers. However, the linear divergence corresponds to the Gamma function at $\Gamma(-1/2)$, which is a finite value. According to dimensional analysis, both the two-loop correction and even higher-loop corrections are linearly divergent. Therefore, in dimensional regularization, the gauge field strength is not renormalized, and $Z_{\rm A}=1$. The same conclusion holds in other renormalization methods.[19] Since $Z_{\rm e}Z_{\rm A}^{1/2}=1$, the charge e is not renormalized, and $Z_{\rm e}=1$. Furthermore, the dielectric constant and magnetic permeability are also not renormalized, and of course, the speed of light is unaffected. This is different from the usual (3+1)-dimensional quantum electrodynamics (QED), where the aforementioned physical quantities are renormalized.[28,31–33] The reason for the difference is that here, the birefringent Dirac fermions are confined to a (2+1)-dimensional spacetime, while the electromagnetic field still exists in (3+1)-dimensional spacetime.

Since $Z_{\rm e}=1$ holds for all orders of perturbation theory, the β-function for e is identically zero, which leads to a trivial RG flow equation for coupling constant, contrasting with standard QED.

4. Renormalization group analysis

The one-loop self-energy corrections lead to renormalization constants that characterize how quantum fluctuations modify the bare parameters of the theory. From these renormalization constants, we can derive the coupled differential equations describing the energy scale dependence of the physical parameters:

$$\begin{aligned}\mu\frac{\mathrm{d}v}{\mathrm{d}\mu}&=-\frac{g^2v}{16\pi^2c}\left\{\left[3-6(1+\beta^2)\frac{v^2}{c^2}\right]F_1\right.\\&\quad+\left[1+2(1-\beta^2)\frac{v^2}{c^2}-4(1+\beta^4)\frac{v^4}{c^4}\right]F_2\\&\quad\left.+4(1-\beta^2)\frac{v^2}{c^2}F_3\right\},\\\mu\frac{\mathrm{d}\beta}{\mathrm{d}\mu}&=\frac{g^2\beta}{16\pi^2c}4(1-\beta^2)\frac{v^2}{c^2}[F_2+2F_3],\end{aligned}\tag{15}$$

where the explicit expressions for $F_1(v,\beta)$, $F_2(v,\beta)$, and $F_3(v,\beta)$ are given in Appendix A. The coupled renormalization group flow equations (15) can be solved numerically. We analyze the flow behavior by considering different sets of initial bare parameters: $(0.3,0.5)$, $(0.5,0.7)$, $(0.8,0.7)$, and $(1.2,0.5)$ [Figs. 3(a)–3(d)]. As the scale parameter l increases (energy scale decreases), we observe that the average Fermi velocity v increases monotonically and asymptotically approaches the speed of light,[19,32] regardless of the initial conditions. This demonstrates the robust emergence of Lorentz symmetry under coarse graining. Furthermore, both β and βv flow monotonically to zero as the energy scale decreases, indicating that in the deep infrared regime, the birefringent pseudospin-3/2 Dirac fermions transform into two degenerate pseudospin-1/2 Dirac fermions.[25,26] This transformation highlights the special status of relativistic spin-1/2 Dirac fermions in low-energy field theories. Notably, while some bare average Fermi velocities in our analysis exceed the speed of light in the medium, the flow towards the speed of light in the infrared limit underscores the robustness of this infrared fixed point. This result provides an indirect explanation for the prevalence of spin-1/2 fermions in the standard model, which is essentially a low-energy theory.

We now study the behavior of the fermion Green's function at the fixed point and consider the Callan–Symanzik equation for the renormalized electron Green's function[34]

$$\begin{aligned}&\left(\frac{\partial}{\partial\ln\mu}+\frac{\mathrm{d}v}{\mathrm{d}\ln\mu}\frac{\partial}{\partial v}+\frac{\mathrm{d}\beta}{\mathrm{d}\ln\mu}\frac{\partial}{\partial\beta}\right.\\&\left.+\frac{\mathrm{d}g}{\mathrm{d}\ln\mu}\frac{\partial}{\partial g}+\frac{\mathrm{d}\ln Z_\Psi}{\mathrm{d}\ln\mu}\right)G(\mathrm{i}\omega,\boldsymbol{k})=0,\end{aligned}\tag{16}$$

where $\mathrm{d}\ln Z_\Psi/\mathrm{d}\ln\mu=g^2/12\pi^2\equiv\eta$, η is the anomalous dimension of the birefringent Dirac fermion field. At the fixed point of the renormalization group flow, the Callan–Symanzik

equation becomes

$$\left(\frac{\partial}{\partial \ln \mu}+\eta\right) G^*(\mathrm{i}\omega,\boldsymbol{k})=0. \tag{17}$$

To preserve the canonical dimension of the electron Green's function, $[E]^{-1}$, the solution is[19,34,35]

$$G^*(\mathrm{i}\omega,0)\sim\frac{1}{\omega^{1-\eta}}. \tag{18}$$

Therefore, the birefringent Dirac fermion field acquires a finite anomalous dimension η, and the quasiparticle residue $Z_\Psi\sim\mu^\eta$. As the energy scale approaches zero, the quasiparticle residue vanishes with a power law, this indicates that the system exhibits non-Fermi liquid behavior at this fixed point.

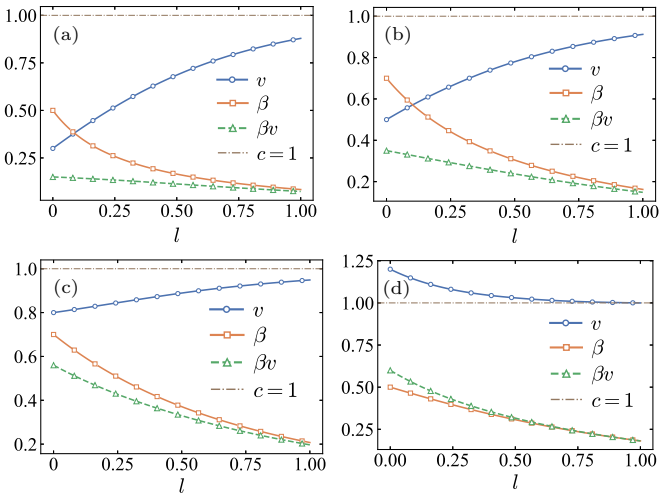


Fig. 3. Renormalization group (RG) flow of the average Fermi velocity (v), birefringence parameter (β), and their product βv for (2+1)-dimensional quasi-relativistic birefringent fermions in the presence of full electromagnetic interactions. Initial conditions are (a) $v_0=0.3$, $\beta_0=0.5$; (b) $v_0=0.5$, $\beta_0=0.7$; (c) $v_0=0.8$, $\beta_0=0.7$; (d) $v_0=1.2$, $\beta_0=0.5$. As the RG scale $l=\frac{3g^2}{16\pi^2}\ln(\Lambda/\mu)$ increases, the average Fermi velocity v approaches the speed of light c, while both the birefringence parameter and the birefringence-induced Fermi velocity difference βv asymptotically approach zero, where we set $c=1$.

The quasiparticle residue Z_Ψ can be defined alternatively as $[1-\frac{\partial}{\partial\omega}\mathrm{Re}\,\Sigma^{\mathrm{R}}]^{-1}$,[36,37] where $\Sigma^{\mathrm{R}}(\omega,\boldsymbol{k})$ is the retarded Green's function, which can be obtained by the analytic continuation of the imaginary-time Green's function, $\Sigma^{\mathrm{R}}(\omega,\boldsymbol{k})=\Sigma(\mathrm{i}\omega\to\omega+\mathrm{i}\delta,\boldsymbol{k})$, δ is a innitesimal positive quantity,[35,38] it can be verified that this definition of the quasiparticle residue is consistent with Z_Ψ [Eq. (11)] obtained as a counterterm at the one-loop level

$$\begin{aligned}&\frac{\partial}{\partial\omega}\mathrm{Re}\,\Sigma^{\mathrm{R}}\\&=\frac{3g^2}{16\pi^2c}\frac{1}{\epsilon}\int_0^1\mathrm{d}x\int_0^{1-x}\mathrm{d}y\frac{\sqrt{1-x-y}}{f(x,y)}\\&\times\left[1-2(1+\beta^2)\frac{v^2}{c^2}+\frac{2(1+\beta^2)\frac{v^2}{c^2}-4(1+\beta^4)\frac{v^4}{c^4}}{3f(x,y)}\right].\end{aligned} \tag{19}$$

Keep terms up to g^2 order, $[1-\frac{\partial}{\partial\omega}\mathrm{Re}\,\Sigma^{\mathrm{R}}]^{-1}=Z_\Psi$.

4.1. No birefringent limit

To compare our work with Refs. [19,20,28], let us take the limit $\beta\to0$ ($c=1$)

$$\begin{aligned}\lim_{\beta\to0}F_1&=-\frac{2}{3(1-v^2)}+\frac{2}{(1-v^2)^2}-\frac{2v}{(1-v^2)^{5/2}}\arccos v,\\\lim_{\beta\to0}F_2&=-\frac{3}{(1-v^2)^2}+\frac{1+2v^2}{v(1-v^2)^{5/2}}\arccos v,\\\lim_{\beta\to0}F_3&=\frac{1}{2(1-v^2)^2}+\frac{1}{4v^2(1-v^2)^2}\\&\quad+\frac{(1/4)-v^2}{v^3(1-v^2)^{5/2}}\arccos v.\end{aligned} \tag{20}$$

Substituting these functions back into Eq. (15), we obtain

$$\mu\frac{\mathrm{d}v}{\mathrm{d}\mu}=-\frac{g^2}{8\pi^2}v\left[\frac{1-4v^2}{1-v^2}+\frac{1}{v}\frac{1-2v^2+4v^4}{(1-v^2)^{3/2}}\arccos v\right]. \tag{21}$$

This result is exactly the same as that in Refs. [19,20,28].

4.2. Non-relativistic limit

Next, we will perform the non-relativistic approximation of the renormalization group flow equations. To better compare our results with the non-relativistic approximation, we define $w=\beta v$ and study the flow of v and w. This approach reflects the symmetry of the system, as the exchange of v and w leaves the system invariant.

$$\begin{aligned}\mu\frac{\mathrm{d}v}{\mathrm{d}\mu}&=-\frac{g^2}{16\pi^2}\frac{v}{c}\left\{\left[3-6\left(\frac{v^2}{c^2}+\frac{w^2}{c^2}\right)\right]F_1\right.\\&\quad+\left[1+2\left(\frac{v^2}{c^2}-\frac{w^2}{c^2}\right)-4\left(\frac{v^4}{c^4}+\frac{w^4}{c^4}\right)\right]F_2\\&\quad\left.+4\left(\frac{v^2}{c^2}-\frac{w^2}{c^2}\right)F_3\right\},\\\mu\frac{\mathrm{d}w}{\mathrm{d}\mu}&=-\frac{g^2}{16\pi^2}\frac{w}{c}\left\{\left[3-6\left(\frac{v^2}{c^2}+\frac{w^2}{c^2}\right)\right]F_1\right.\\&\quad+\left[1-2\left(\frac{v^2}{c^2}-\frac{w^2}{c^2}\right)-4\left(\frac{v^4}{c^4}+\frac{w^4}{c^4}\right)\right]F_2\\&\quad\left.-4\left(\frac{v^2}{c^2}-\frac{w^2}{c^2}\right)F_3\right\}.\end{aligned} \tag{22}$$

In the non-relativistic limit, both the ratios of the Fermi velocity to the speed of light v/c and w/c approach zero. Perform a small expansion on the right-hand side of the system of equations, the above equation becomes

$$\mu\frac{\mathrm{d}v}{\mathrm{d}\mu}=-\frac{g^2}{16\pi},\quad\mu\frac{\mathrm{d}w}{\mathrm{d}\mu}=0. \tag{23}$$

The above equation is valid for $v>w$. If $v<w$, then the equation becomes

$$\mu\frac{\mathrm{d}v}{\mathrm{d}\mu}=0,\quad\mu\frac{\mathrm{d}w}{\mathrm{d}\mu}=-\frac{g^2}{16\pi}. \tag{24}$$

In the non-relativistic limit ($c\to\infty$), the average Fermi velocity v increases with the logarithm of the energy scale,

while the birefringence parameter β decreases with the logarithm of the energy scale, their product w remains invariant under the renormalization scale changes. This result is the same as that in Ref. [25]. Figure 4(a) is the renormalization flow diagram in the non-relativistic limit, when v increases to a value comparable to the speed of light, the non-relativistic approximation breaks down, as shown in Fig. 4(b), w starts to decrease, and eventually v reaches the speed of light while w goes to zero. If the initial conditions of v and w are swapped, their flows will also swap; in other words, the larger of v and w will reach the speed of light, and the smaller will approach zero. Eventually, the birefringent Dirac fermion transforms into two decoupled relativistic pseudospin-1/2 Dirac fermions. Notably, there are two fixed points in Fig. 4(b): $v=1, w=0$ and $w=1, v=0$. However, these represent the same fixed point, as the cases $v>w$ and $v<w$ are physically equivalent, different representations of the Dirac matrices are physically equivalent.

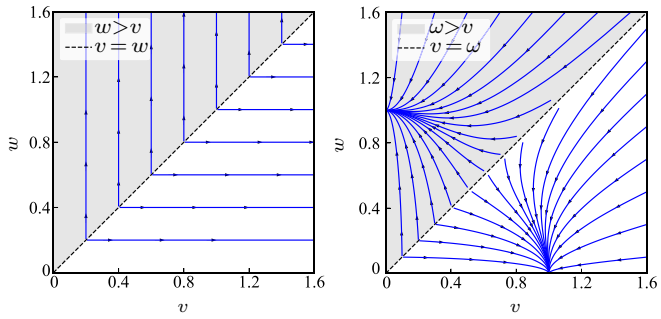


Fig. 4. RG flow of the velocity v and birefringence parameter β under the influence of long-range Coulomb interactions for (a) non-relativistic limit ($c\to\infty$) and (b) relativistic case ($c=1$). The shaded regions indicate where the birefringence parameter exceeds unity ($\beta>1$). The flow diagram reveals two infrared stable fixed points at $(v,w)=(1,0)$ and $(v,w)=(0,1)$, where $w=\beta v$.

By analytically solving the double integral of the renormalization group β-function, we found that $v=w$, i.e., $\beta=1$ causes the denominator of some expressions in the β-function to vanish, a singularity appears in the renormalization group flow equations, indicating that our theory cannot capture the physics at $\beta=1$. It is worth noting that when $\beta=1$, the energy spectrum of the birefringent Dirac fermions is no longer two nested Dirac cones, but rather one Dirac cone plus two flat bands. It is possible that the $\beta=1$ case can be captured by considering k^2 corrections in the derivation of the effective Hamiltonian, and we leave this investigation for future work.

5. Discussion and conclusion

In this work, we have explored the low energy behavior of interacting quasi-relativistic spin-3/2 birefringent Dirac fermions, emphasizing the impact of long-range Coulomb interactions and retarded current–current interactions among fermions. Our principal finding is that at the infrared fixed point of the renormalization group (RG) flow, the low-energy dynamics of the system can be effectively characterized as a non-Fermi liquid composed of relativistic pseudospin-1/2 Dirac fermions, where the fermion field exhibits a finite anomalous dimension and the residue of the quasiparticle pole vanishes in a power-law fashion. Our analysis can be generalized to encompass quasi-relativistic Dirac fermions with higher odd spins and multiple refractive indices. This universality implies a more fundamental principle governing the low energy behavior of fermionic systems with multiple characteristic velocities. The emergence of pseudospin-1/2 fermions at low energies has significant implications for particle physics, particularly concerning the standard model, where all fundamental fermions possess spin-1/2 and are understood as a low-energy effective theory relative to its cutoff scale. This suggests a potential deeper connection between the emergence of spin-1/2 fermions and fundamental symmetries in nature. Looking ahead, a critical extension of our work would involve examining the coupling between quasi-relativistic birefringent Dirac fermions and their environment through explicit non-Hermitian terms in the Hamiltonian operator. Specifically, it remains to be determined whether the non-Fermi liquid behavior persists in non-Hermitian birefringent Dirac semimetals, a topic reserved for future investigation.

Appendix A: Vertex correction and Ward identity

In this appendix, we calculate the vertex correction Feynman diagram for Fig. 2(b). We only compute the divergent part of the Feynman diagram, and since the external momentum is independent of the divergent part, we set the external momentum to zero for convenience,[19] thereby omitting the tedious algebraic calculations, the one-loop vertex correction is $(c=1)$

$$
\begin{aligned}
\boldsymbol{V}_0 &= e^3\int\frac{\mathrm{d}^3k}{(2\pi)^3}\gamma_\rho S(k)\gamma_0 S(k)\gamma_\nu \tilde{D}_{\nu\rho}(k)\\
&= \frac{\mathrm{i}e^3}{2\varepsilon}\int\frac{\mathrm{d}^3k}{(2\pi)^3}\frac{\gamma_\rho[\mathrm{i}k_0+H][k_0^2+(1+\beta^2)v^2|\boldsymbol{k}|^2-2\beta v^2H_1H_2][\mathrm{i}k_0+H][k_0^2+(1+\beta^2)v^2|\boldsymbol{k}|^2-2\beta v^2H_1H_2]\gamma_\rho}{[k_0^2+(1+\beta)^2v^2|\boldsymbol{k}|^2]^2[k_0^2+(1-\beta)^2v^2|\boldsymbol{k}|^2]^2\sqrt{k_0^2+k_1^2+k_2^2}}\\
&= \frac{15\mathrm{i}e^3}{64\pi^2\varepsilon}\left[\frac{1}{\epsilon}+O(\epsilon^0)\right]\int_0^1\mathrm{d}x\int_0^{1-x}\mathrm{d}y\frac{xy}{\sqrt{1-x-y}}\frac{1}{f(x,y)}
\end{aligned}
$$

$$\times\left\{\left[1+\frac{2(1+\beta^2)v^2}{5f}-\frac{8(1-10\beta^2+\beta^4)v^4}{15f^2}-\frac{16(1-\beta^2)(1-\beta^4)v^6}{5f^3}\right]\left[1-2(1+\beta^2)v^2-2\beta v^2(\Gamma_{11}+\Gamma_{22})\right]\right.$$
$$\left.+\left[\frac{6\beta v^2}{5f}+\frac{16\beta(1+\beta^2)v^4}{15f^2}-\frac{16\beta(1-\beta^2)^2v^6}{5f^3}\right]\left[4\beta v^2(1+\Gamma_{33})-(\Gamma_{11}+\Gamma_{22})\right]\right\}, \tag{A1}$$

$$\begin{aligned}\boldsymbol{V}_j &= e^3\int\frac{\mathrm{d}^3k}{(2\pi)^3}\gamma_\rho S(k)\gamma_j S(k)\gamma_\nu\tilde{D}_{\nu\rho}(k)\\ &=\frac{e^3}{2\varepsilon}\int\frac{\mathrm{d}^3k}{(2\pi)^3}\frac{\gamma_\rho[\mathrm{i}k_0+H][k_0^2+(1+\beta^2)v^2|\boldsymbol{k}|^2-2\beta v^2H_1H_2]\gamma_j[\mathrm{i}k_0+H][k_0^2+(1+\beta^2)v^2|\boldsymbol{k}|^2-2\beta v^2H_1H_2]\gamma_\rho}{[k_0^2+(1+\beta)^2v^2|\boldsymbol{k}|^2]^2[k_0^2+(1-\beta)^2v^2|\boldsymbol{k}|^2]^2\sqrt{k_0^2+k_1^2+k_2^2}}\\ &=\frac{15e^3}{64\pi^2\varepsilon}\left[\frac{1}{\epsilon}+O(\epsilon^0)\right]\int_0^1\mathrm{d}x\int_0^{1-x}\mathrm{d}y\frac{xy}{\sqrt{1-x-y}}\frac{1}{f(x,y)}\\ &\quad\times\left\{\left[1-4\beta^2v^2+\frac{4(1-\beta^2)v^2}{5f}+\frac{16(1-\beta^4)v^4}{15f^2}-\frac{8(1-\beta^2)^2v^4(1-4\beta^2v^2)}{15f^2}\right]v\Gamma_{j0}\right.\\ &\quad\left.+\left[1-4v^2-\frac{4(1-\beta^2)v^2}{5f}-\frac{16(1-\beta^4)v^4}{15f^2}-\frac{8(1-\beta^2)^2v^4(1-4v^2)}{15f^2}\right]\beta v\Gamma_{0j}\right\},\quad(j=1,2).\end{aligned} \tag{A2}$$

The Ward identity we aim to prove is the following relationship between the fermion self-energy correction and the vertex correction:[28,39]

$$\frac{\partial\Sigma(\mathrm{i}\Omega,\boldsymbol{p})}{\partial\Omega}=-\frac{1}{e}\boldsymbol{V}_0,\quad\frac{\partial\Sigma(\mathrm{i}\Omega,\boldsymbol{p})}{\partial p_j}=-\frac{c}{e}\boldsymbol{V}_j,\quad j=1,2. \tag{A3}$$

To prove the above equation, we combine Eq. (9) with Eqs. (A1) and (A2) and do a slight rearrangement, and then we can obtain

$$\begin{aligned}&\frac{\partial\Sigma(\mathrm{i}\Omega,\boldsymbol{p})}{\partial\Omega}+\frac{\boldsymbol{V}_0}{e}=\frac{3\mathrm{i}e^2}{16\pi^2\varepsilon}\frac{1}{\epsilon}\left[H_1(v,\beta)[1-2(1+\beta^2)v^2-2\beta v^2(\Gamma_{11}+\Gamma_{22})]+H_2(v,\beta)[4\beta v^2(1+\Gamma_{33})-(\Gamma_{11}+\Gamma_{22})]\right],\\ &\frac{\partial\Sigma(\mathrm{i}\Omega,\boldsymbol{p})}{\partial p_j}+\frac{c}{e}\boldsymbol{V}_j=-\frac{3e^2}{16\pi^2\varepsilon}\frac{1}{\epsilon}\left[H_3(v,\beta)v\Gamma_{j0}+H_4(v,\beta)\beta v\Gamma_{0j}\right],\quad j=1,2.\end{aligned} \tag{A4}$$

By proving that the four functions $H_1(v,\beta)$, $H_2(v,\beta)$, $H_3(v,\beta)$, and $H_4(v,\beta)$ are identically zero, we can directly prove the above Ward identity. The specific expressions of these four functions are as follows:

$$\begin{aligned}H_1(v,\beta)&=F_1+\frac{2}{3}(1+\beta^2)v^2F_2+\frac{5}{4}G_1+\frac{1}{2}(1+\beta^2)v^2G_2-\frac{2}{3}(1-10\beta^2+\beta^4)v^4G_3-4(1-\beta^2)(1-\beta^4)v^6G_4,\\ H_2(v,\beta)&=\frac{2}{3}\beta v^2F_2+\frac{3}{2}\beta v^2G_2+\frac{4}{3}\beta(1+\beta^2)v^4G_3-4\beta(1-\beta^2)^2v^6G_4,\\ H_3(v,\beta)&=\frac{1-4\beta^2v^2}{3}F_2+\frac{4}{3}(1-\beta^2)v^2F_3-\left(\frac{5}{4}-5\beta^2v^2\right)G_1-(1-\beta^2)v^2G_2-\frac{4}{3}(1-\beta^4)v^4G_3+\frac{2}{3}(1-\beta^2)^2v^4(1-4\beta^2v^2)G_3,\\ H_4(v,\beta)&=\frac{1-4v^2}{3}F_2-\frac{4}{3}(1-\beta^2)v^2F_3-\left(\frac{5}{4}-5v^2\right)G_1+(1-\beta^2)v^2G_2+\frac{4}{3}(1-\beta^4)v^4G_3+\frac{2}{3}(1-\beta^2)^2v^4(1-4v^2)G_3,\end{aligned} \tag{A5}$$

where

$$F_n(v,\beta)=\int_0^1\mathrm{d}x\int_0^{1-x}\mathrm{d}y\frac{\sqrt{1-x-y}}{f^n(x,y)},\quad G_n(v,\beta)=\int_0^1\mathrm{d}x\int_0^{1-x}\mathrm{d}y\frac{xy}{f^n(x,y)\sqrt{1-x-y}}, \tag{A6}$$

F_n and G_n can be integrated out. Define $a=1-(1+\beta)^2v^2$, $b=1-(1-\beta)^2v^2$. Below are the explicit expressions for F_1, F_2, F_3, G_1, G_2, G_3, G_4:

$$\begin{aligned}F_1&=\frac{4}{3}\frac{1}{ab}+\frac{4}{3}\frac{1}{b-a}\left[\frac{(1-b)}{b}\sqrt{\frac{1-b}{b}}\arctan\sqrt{\frac{b}{1-b}}-\frac{(1-a)}{a}\sqrt{\frac{1-a}{a}}\arctan\sqrt{\frac{a}{1-a}}\right],\\ F_2&=-2\frac{1}{ab}-2\frac{1}{b-a}\left[\frac{1}{b}\sqrt{\frac{1-b}{b}}\arctan\sqrt{\frac{b}{1-b}}-\frac{1}{a}\sqrt{\frac{1-a}{a}}\arctan\sqrt{\frac{a}{1-a}}\right],\\ F_3&=\frac{1}{2}\frac{1}{ab}+\frac{1}{2}\frac{1}{b-a}\left[\frac{1}{b(1-b)}\sqrt{\frac{1-b}{b}}\arctan\sqrt{\frac{b}{1-b}}-\frac{1}{a(1-a)}\sqrt{\frac{1-a}{a}}\arctan\sqrt{\frac{a}{1-a}}\right],\end{aligned} \tag{A7}$$

$$
\begin{aligned}
G_1 = {} & \frac{2}{(b-a)^3}\left[\frac{2}{3}(b-a)-\frac{4}{15}(b^2-a^2)+(1-a)(1-b)\left(2\sqrt{\frac{1-b}{b}}\arctan\sqrt{\frac{b}{1-b}}-2\sqrt{\frac{1-a}{a}}\arctan\sqrt{\frac{a}{1-a}}\right)\right.\\
& +(a+b-2ab)\left(\frac{2}{3b}-\frac{2}{3a}-\frac{2(1-b)^{3/2}}{3b^{3/2}}\arctan\sqrt{\frac{b}{1-b}}+\frac{2(1-a)^{3/2}}{3a^{3/2}}\arctan\sqrt{\frac{a}{1-a}}\right)\\
& \left.+ab\left(\frac{14}{15b}-\frac{14}{15a}-\frac{2}{5b^2}+\frac{2}{5a^2}+\frac{2(1-b)^{5/2}}{5b^{5/2}}\arctan\sqrt{\frac{b}{1-b}}-\frac{2(1-a)^{5/2}}{5a^{5/2}}\arctan\sqrt{\frac{a}{1-a}}\right)\right],\\
G_2 = {} & \frac{2}{(b-a)^3}\left[\frac{4}{3}(a-b)+\frac{2b}{3a}-\frac{2a}{3b}+\left[(a+b)\left(\frac{2}{3b}+\frac{4}{3}\right)-4\right]\sqrt{\frac{1-b}{b}}\arctan\sqrt{\frac{b}{1-b}}\right.\\
& \left.-\left[(a+b)\left(\frac{2}{3a}+\frac{4}{3}\right)-4\right]\sqrt{\frac{1-a}{a}}\arctan\sqrt{\frac{a}{1-a}}\right],\\
G_3 = {} & \frac{1}{(b-a)^3}\left[\frac{a}{b}-\frac{b}{a}+\frac{5b-4b^2-a}{b^{3/2}(1-b)^{1/2}}\arctan\sqrt{\frac{b}{1-b}}-\frac{5a-4a^2-b}{a^{3/2}(1-a)^{1/2}}\arctan\sqrt{\frac{a}{1-a}}\right],\\
G_4 = {} & \frac{1}{(b-a)^3}\left[\frac{(a-5b-2ab+6b^2)}{6b^{3/2}(1-b)^{3/2}}\arctan\sqrt{\frac{b}{1-b}}-\frac{(b-5a-2ab+6a^2)}{6a^{3/2}(1-a)^{3/2}}\arctan\sqrt{\frac{a}{1-a}}+\frac{b-a}{6b(1-b)}-\frac{a-b}{6a(1-a)}\right]. \qquad \text{(A8)}
\end{aligned}
$$

Figure A1 shows the values of H_1, H_2, H_3, H_4 as functions of v and β. It can be seen that they are all zero. The singularities at $v=0$ and $\beta=1$ arise because they cause certain denominators in the functions F_1, F_2, F_3, G_1, G_2, G_3, G_4 to become zero, and the numerical precision of the plot is limited.

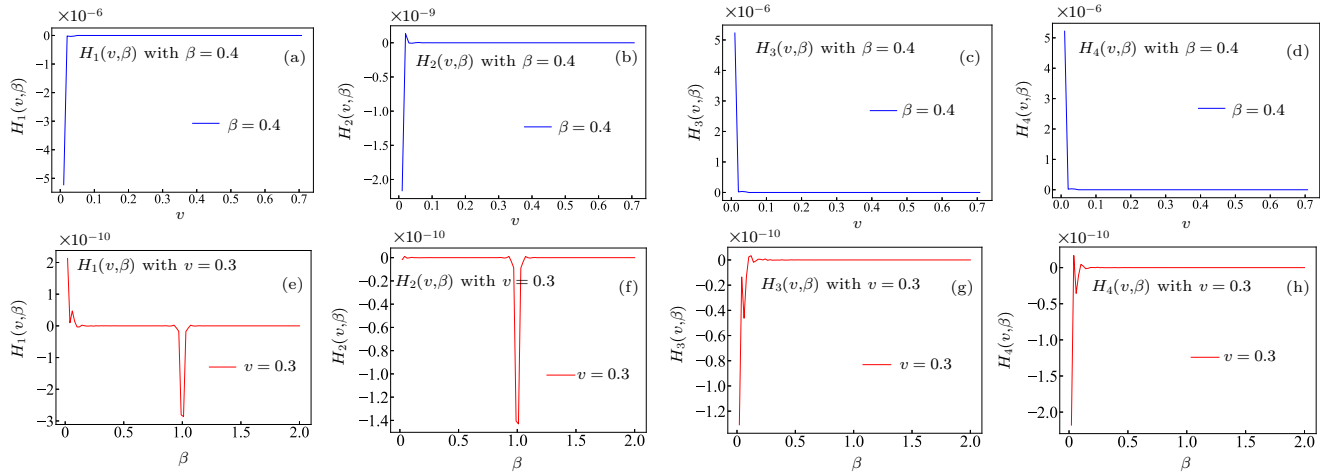


Fig. A1. The functions $H_j(v,\beta)$, $j=1,2,3,4$ as functions of v and β. (a) H_1 as a function of v when $\beta=0.4$, (b) H_2 as a function of v when $\beta=0.4$, (c) H_3 as a function of v when $\beta=0.4$, (d) H_4 as a function of v when $\beta=0.4$, (e) H_1 as a function of β when $v=0.3$, (f) H_2 as a function of β when $v=0.3$, (g) H_3 as a function of β when $v=0.3$, (h) H_4 as a function of β when $v=0.3$.

Acknowledgements

Project supported by the National Key Research and Development Program of China (Grant Nos. 2021YFA1400900, 2021YFA0718300, and 2021YFA1400243), the National Natural Science Foundation of China (Grant Nos. 61835013, 12174461, and 12234012), and Space Application System of China Manned Space Program.

References

[1] Liu Z H, Vojta M, Assaad F F and Janssen L 2022 *Phys. Rev. Lett.* **128** 087201
[2] Boyack R, Yerzhakov H and Maciejko J 2021 *Euro. Phys. J. Spec. Top.* **230** 979
[3] Schwab J, Janssen L, Sun K, Meng Z Y, Herbut I F, Vojta M and Assaad F F 2022 *Phys. Rev. Lett.* **128** 157203
[4] Hao Y, Pan G, Sun K, Meng Z Y and Qi Y 2022 *Chin. Phys. Lett.* **39** 097102
[5] Hou Q, Song M, Xu X, Wang Y, Dong C, Feng Y, He M, Liu Y, Cao L, Wang J, *et al.* 2023 *Chin. Phys. B* **32** 087501
[6] Jian S K and Yao H 2017 *Phys. Rev. B* **96** 195162
[7] Roy B, Goswami P and Juričić V 2018 *Phys. Rev. B* **97** 205117
[8] Kennett M P, Komeilizadeh N, Kaveh K and Smith P M 2011 *Phys. Rev. A* **83** 053636
[9] Roy B, Smith P M and Kennett M P 2012 *Phys. Rev. B* **85** 235119
[10] Komeilizadeh N and Kennett M P 2014 *Phys. Rev. B* **90** 045131
[11] Guo H M, Wang L and Scalettar R 2018 *Phys. Rev. B* **97** 235152
[12] Wang Y X and Li F 2019 *Phys. Rev. B* **99** 245126
[13] Teber S 2012 *Phys. Rev. D* **86** 025005
[14] Kotikov A and Teber S 2014 *Phys. Rev. D* **89** 065038
[15] Kotikov A and Teber S 2016 *Phys. Rev. D* **94** 114010
[16] Alves V S, Junior R O, Marino E and Nascimento L O 2017 *Phys. Rev. D* **96** 034005
[17] Magalhães G C, Alves V S, Marino E C and Nascimento L O 2020 *Phys. Rev. D* **101** 116005

[18] Fernández L, Alves V S, Nascimento L O, Peña F, Gomes M and Marino E 2020 *Phys. Rev. D* **102** 016020

[19] González J, Guinea F and Vozmediano M 1994 *Nucl. Phys. B* **424** 595

[20] Isobe H and Nagaosa N 2016 *Coulomb interaction effect in tilted Weyl fermion in two dimensions*, APS March Meeting Abstracts, Vol. 2016 pp. S13–003

[21] Aidelsburger M, Atala M, Lohse M, Barreiro J T, Paredes B and Bloch I 2013 *Phys. Rev. Lett.* **111** 185301

[22] Sørensen A S, Demler E and Lukin M D 2005 *Phys. Rev. Lett.* **94** 086803

[23] Dagotto E, Fradkin E and Moreo A 1986 *Phys. Lett. B* **172** 383

[24] Murshed S A and Roy B 2024 arXiv preprint arXiv: 2407.18250

[25] Roy B, Kennett M P, Yang K and Juričić V 2018 *Phys. Rev. Lett.* **121** 157602

[26] Roy B and Juričić V 2020 *Phys. Rev. Res.* **2** 012047

[27] Peskin M E 2018 *An introduction to quantum field theory* (CRC Press)

[28] Murshed S A and Roy B 2024 *J. High Energy Phys.* **2024** 143

[29] Carrington M 2019 *Phys. Rev. B* **99** 115432

[30] Veltman M *et al.* 1972 *Nucl. Phys. B* **44** 189

[31] Isobe H and Nagaosa N 2012 *Phys. Rev. B* **86** 165127

[32] Roy B, Juričić V and Herbut I F 2016 *J. High Energy Phys.* **2016** 18

[33] Pozo O, Ferreiros Y and Vozmediano M A 2018 *Phys. Rev. B* **98** 115122

[34] Srednicki M 2007 *Quantum field theory* (Cambridge University Press)

[35] Isobe H and Fu L 2019 *Phys. Rev. Res.* **1** 033206

[36] Nayak C and Wilczek F 1994 *Nucl. Phys. B* **417** 359

[37] Bruus H and Flensberg K 2004 *Many-body quantum theory in condensed matter physics: an introduction* (OUP Oxford)

[38] Sachdev S 2024 arXiv:2407.15919 [cond-mat.str-el]

[39] Ward J C 1950 *Phys. Rev.* **78** 182